



# Influence of fabrication deviations on the polarization-maintaining behavior of inhibited-coupling guiding hollow-core fibers

Bowen Chen<sup>1,2</sup> · Tim Kühnthau<sup>1</sup> · Christian Röhler<sup>1</sup> · Thomas Graf<sup>1</sup> · Marwan Abdou Ahmed<sup>1</sup>

Received: 19 October 2023 / Accepted: 28 March 2024 / Published online: 18 April 2024  
© The Author(s) 2024

## Abstract

Numerical simulations were conducted to analyze the influence of the design parameters of tubular inhibited-coupling guiding hollow-core photonic crystal fibers (IC-HCPCFs) on the bending-induced phase shift. The possibility to implement polarization-maintaining (PM) tubular IC-HCPCFs using a low-birefringence approach (with a modal birefringence parameter  $B < 7 \times 10^{-9}$ ) is discussed. Two different tubular IC-HCPCF designs with 7 and 8 glass capillaries are proposed for operation at a wavelength of 1030 nm. The numerical simulation predicts low guiding losses and a PM behavior sustaining a degree of linear polarization (DOLP) larger than 90% after 10 m of fiber with a bend radius larger than 0.2 m. This shows great potential for high-power beam delivery in an industrial environment. The influence that fabrication deviations have on the polarization-maintaining behavior was also investigated and indicates tight fabrication tolerances for both proposed fiber designs. Small deviations from the ideal symmetrical structure can lead to an enhancement of undesired modal birefringence. To ensure a DOLP larger than 90% at the exit of a 10 m-long fiber and for a bending radius  $> 0.2$  m precise control of the drawing parameters during the fiber production is required, which is challenging but is considered to be technically feasible.

## 1 Introduction

The flexible guiding of light in air-filled hollow-core fibers over long distances has been of interest already for several decades due to the inherently low absorption and dispersion of this kind of fiber [1, 2]. Low losses [3], tunable dispersion [4], and effective single-modeness [5] can be achieved using photonic bandgap hollow-core photonic crystal fibers (PBG-HCPCFs) [6]. The drawbacks of PBG-HCPCFs are however a comparatively narrow transmission bandwidth [7] and a high overlap of the core-guided mode with the surrounding glass [8], which limits the applications of this kind of fibers. An alternative hollow-core fiber concept is that of the inhibited-coupling guiding hollow-core photonic crystal fibers (IC-HCPCFs) which were introduced by [9]. Thanks to their low confinement losses [10], low dispersion [11], broad transmission bandwidth [12], high laser-induced

damage threshold [13], and the possibility of effective single-mode guidance [14], IC-HCPCFs show great potential in data transmission [15], gas photonics [16], quantum communication [17], optical sensing [18], and high-power beam delivery [19].

The development of ultrafast lasers with high energies and high peak powers has enabled numerous applications in material processing, such as precise drilling of holes with high aspect ratios and minimal heat-affected zone [20], high-quality and high-throughput cutting of carbon-fiber reinforced composites [21] and surface structuring [22, 23]. In this kind of application, IC-HCPCFs are seen as an ideal means for the flexible delivery of ultrashort laser pulses due to their capability to handle high powers and intensities [24]. During beam delivery, it is always desirable to preserve all the important properties of the laser beam, including temporal pulse shape, spectral width, peak power, and especially the state of polarization, since the latter plays an essential role in many of the processes [25].

Conventional solid-core fibers with circular symmetrical structures are not polarization-maintaining since any inhomogeneity of the profile of the refractive index and deviations from the perfect circular geometry of the fiber lead to random differences in the propagation constants of the two orthogonally polarized fundamental modes, thus resulting in

✉ Bowen Chen  
bowen.chen@ifsw.uni-stuttgart.de

<sup>1</sup> Institut für Strahlwerkzeuge (IFSW), University of Stuttgart, Pfaffenwaldring 43, 70569 Stuttgart, Germany

<sup>2</sup> Graduate School of Excellence advanced Manufacturing Engineering (GSaME), University of Stuttgart, Nobelstraße 12, 70569 Stuttgart, Germany

a degradation of the polarization state [26]. The difference in the propagation constants between the two orthogonally polarized fundamental modes can intentionally be enlarged by using stress rods or applying elliptical core shapes [27]. This high modal birefringence provokes a periodical change of the polarization state which can therewith be maintained for a given fiber length [28].

The approach to enlarge the modal birefringence using elliptical cores to maintain the polarization state in the fiber has also been adopted for HC-PCFs [29]. The difference in the effective refractive indices between the two orthogonally polarized modes was increased by using four elliptical elements surrounding the fiber's core to obtain a PM behavior [30]. Engineering two shunts in the cladding's glass web, high birefringence can be achieved by inducing coupling between one of the polarized modes with surface modes surrounding the fiber's core [31]. The overlap between the core modes and the surrounding glass structures is however increased as well with these concepts, which are therefore not suitable for high-power applications.

High birefringence can be obtained in IC-HCPCFs with an elliptical core shape [32, 33] or by modifying the thickness of the glass strut of the capillaries in the fiber's cladding [34–39]. This is however quite challenging to control by pressurizing the capillaries during fiber production. In the meantime, it has also been proven that even without such intentional modifications, IC-HCPCFs can exhibit a polarization-maintaining behavior due to the ultralow interaction between core and cladding modes inherent to the guiding mechanism [40]. High polarization purity can be achieved due to the low overlap and thus the weak perturbation of the core modes. For a 3-m Kagomé IC-HC-PCF with an optimized hypocycloid-shaped core, a 26 dB maximum polarization extinction ratio (PER) was measured [41]. The polarization-maintaining properties of another tubular IC-HCPCF were reported on in [10] showing a maximum measured PER of 15.5 dB after 16 m of fiber. A high PER larger than 40 dB could be measured through a 33-m long tubular IC-HCPCF without being intentionally designed for high birefringence [40]. The same group demonstrated an even higher measured PER of 69.8 dB after 178 m hollow-core Nested Antiresonant Nodeless Fiber (HC-NANF) and this high polarization purity was robust against temperature changes [40]. Nevertheless, the state of polarization can degrade when the phase shift between the two orthogonally polarized fiber modes is increased due to the bending of the fiber. Due to the low birefringence exhibited by the tubular IC-HCPCF, the polarization mode coupling cannot be avoided by bending the fiber. Thus, the phase shift between the two polarized modes determines the state of the polarization at the output of the fiber. It was shown that the bending-induced phase shift gets larger with diminishing bending radius due to the enhanced polarization mode coupling between the two

orthogonally polarized core modes [42]. When the beam is polarized either parallel or perpendicular to the bending plane of the fiber, it excites only one polarized mode. Both orthogonally polarized fiber modes are excited otherwise. The linear polarization state of the beam is maintained when the phase shift between the two polarized modes is zero. The influence of the design parameters of IC-HCPCFs on the bending-induced phase shift has however not been studied in detail yet.

The influence of key fiber parameters on the bending-induced phase shift, which can lead to a degradation of the polarization state during propagation through tubular IC-HCPCFs, was therefore studied numerically. We present a theoretical analysis of the polarization-maintaining properties of two fiber designs and discuss the impact that fabrication deviations have on the PM behavior of tubular IC-HCPCFs. Although the analysis is devoted to tubular IC-HCPCFs in this report, the same design strategy can also be used for the other fiber structures, such as Kagomé [43], conjoined-tube [44], and nested [2] fibers. Our work concentrates on the application of flexible delivery of fundamental-mode laser beams for material processing. Considering the critical bending losses and laser-induced damage threshold only bending radii larger than 0.2 m [45] were taken into consideration while the wavelength was set to 1030 nm as for beams emitted from Yb: YAG lasers.

## 2 Numerical methods

A simulation model based on the finite-element method (FEM) was implemented using the commercially available software COMSOL Multiphysics to calculate the effective refractive indices  $n_{eff,\parallel}$  and  $n_{eff,\perp}$  of the orthogonally polarized fundamental modes, parallel or perpendicular to the plane of the fiber bending, respectively. The maximum mesh size was set to be  $\leq 0.2$  times the wavelength and the whole fiber cross-section was surrounded by an optimized perfectly matched layer with a thickness of 10  $\mu\text{m}$  [46]. Conformal mapping was implemented to model the effect of fiber bending with different orientations of the bending plane [47].

The geometries of the tubular IC-HCPCFs which were investigated are shown in Fig. 1. The fiber consists of several glass capillaries with thin membranes (blue) forming the cladding structure inside the glass outer cladding (yellow) and a hollow core filled with air. Since the orientation of the bending of tubular IC-HCPCFs was found to have only a limited influence on the resulting phase shift in our previous work [42], only one bending orientation was considered for each fiber design in the present analysis. Fibers with an odd number of capillaries are bent in the plane through the gap between two capillaries and the center of the opposite capillary, while fibers with an even number of capillaries are bent

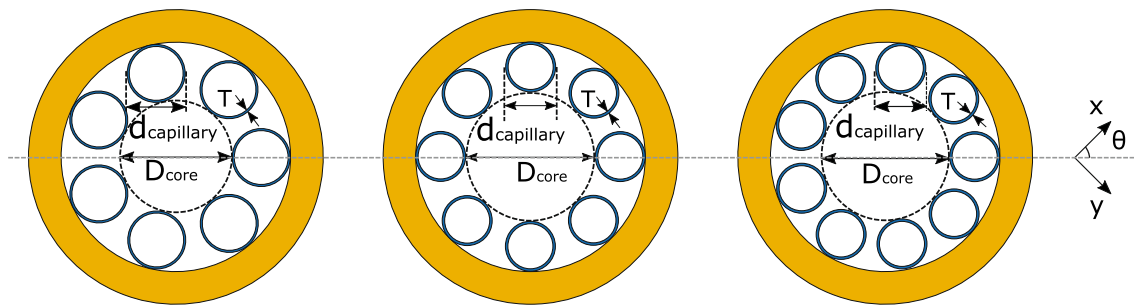


**Fig. 1** a–c Cross-sectional view of tubular IC-HCPCFs with 7, 8 and 9 capillaries. **d** Coordinate system used to characterize the polarization of an incident laser beam launched into the fiber (see later). The dashed horizontal line indicates the plane in which the fibers are bent

in the plane through the center of two opposite capillaries (grey dashed horizontal line). The anti-resonant wavelength of the fiber, which approximately corresponds to the center of the spectral transmission band, can be estimated by [12]

$$\lambda_{anti} = \frac{2T}{(l-0.5)} \sqrt{n_{glass}^2 - n_{air}^2} \quad (1)$$

where  $T$  is the strut thickness of the capillaries,  $l$  is an integer numbering the transmission band (1, 2, 3, ...), and  $n_{glass}$  and  $n_{air}$  are the refractive indices of glass and air, respectively. The phase shift between the two polarized modes can be calculated with

$$\Delta\delta = \frac{2\pi}{\lambda} \Delta n_{eff} = \frac{2\pi}{\lambda} |n_{eff,\parallel} - n_{eff,\perp}| \quad (2)$$

where  $\lambda$  is the wavelength of the light propagating in the fiber [12].

### 3 Influence of key fiber parameters on the polarization-maintaining effect

As a starting point, the initial fiber design was based on the seminal work of Kolyadin [48]. A core diameter of  $D_{core} = 40 \mu\text{m}$  and 8 evenly sized glass capillaries with an outer diameter of  $d_{capillary} = 15.08 \mu\text{m}$  were chosen, see Fig. 1b. The characteristic ratio  $d_{capillary}/D_{core}$  therefore amounts to 0.377. Instead of operating the fiber in the fundamental transmission band as reported in [10], the strut thickness was set to 736 nm, by which the anti-resonant wavelength of 1030 nm comes to lie in the second transmission band. This has the advantages that the fabrication of the fibers is less challenging and that the thicker glass membranes are less susceptible to damage. According to a theoretical analysis in [49], the coupling efficiency between an incident Gaussian beam and the fundamental mode of the fiber is even higher than in the first transmission band, which is

beneficial to suppress the excitation of modes with higher transverse order.

Figure 2 shows the calculated confinement losses averaged between the two orthogonally polarized fundamental modes (left) and the phase shift between them as a function of the wavelength for different bending radii in the plane of two opposite capillaries as specified above (right). As expected, the confinement losses increase with decreasing bending radius. At a wavelength of 1030 nm, they amount to about 8 dB/km in the straight fiber and 9 dB/km when the fiber is bent to a radius of 0.2 m. Still, the spectral bandwidth in which the losses are lower than 15 dB/km is larger than 200 nm, which shows the advantage of tubular IC-HCPCFs for the flexible guiding of ultrashort laser pulses. The phase shift between the two orthogonally polarized modes in the straight fiber is always almost zero in the whole wavelength range, which means that the polarization state of the transmitted beam can be maintained as long as the fiber is not bent. For bent fibers, however, the phase shift first decreases to a minimum value close to zero and then increases again with increasing wavelength. The bending-induced phase shift increases with decreasing bending radius, but the spectral position with minimal phase shift is virtually kept at the same wavelength. Near the spectral position with minimal phase shift, however, the phase shift is only weakly affected by a change of the bend radius. This phenomenon can be attributed to the low interaction between the core-guided modes and modes in the cladding capillaries with high transverse order which constitutes the guidance mechanism of IC-HCPCFs. It is important to note that Eq. 1 is only an approximation for the anti-resonant wavelength. The actual anti-resonant wavelength of the IC-HCPCFs depends not only on the strut thickness but also on the number of the glass capillaries, their diameter, and the core diameter of the fiber. As can be seen from the example in Fig. 2, the actual anti-resonant wavelength of the fiber is approximately 1012 nm and deviates from the 1030 nm calculated with Eq. 1. In the following analysis, it

**Fig. 2 a** Confinement loss averaged over the two orthogonally polarized fundamental modes. **b** Phase shift between the two orthogonally polarized fundamental modes of the fiber structure shown in Fig. 1 with core diameter of 40  $\mu\text{m}$ , 8 evenly sized glass capillaries with an outer diameter of 15.08  $\mu\text{m}$  and glass strut thickness of 736 nm as a function of the wavelength

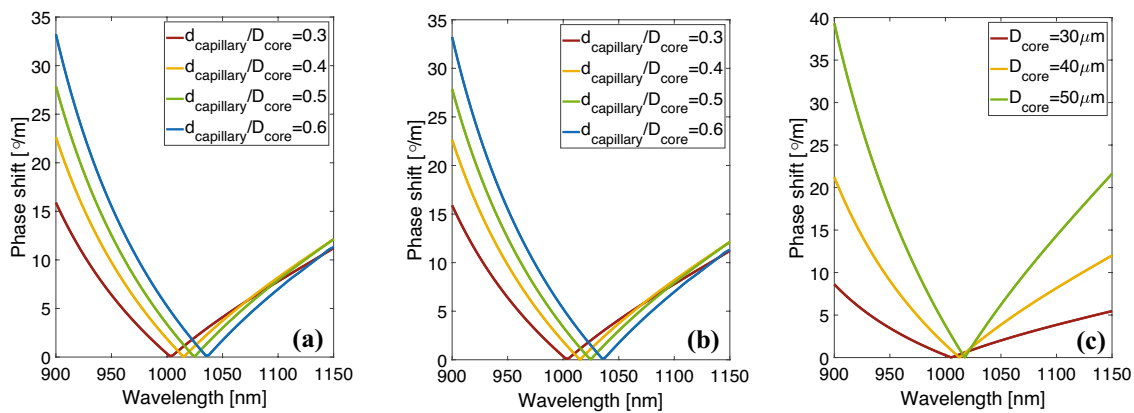
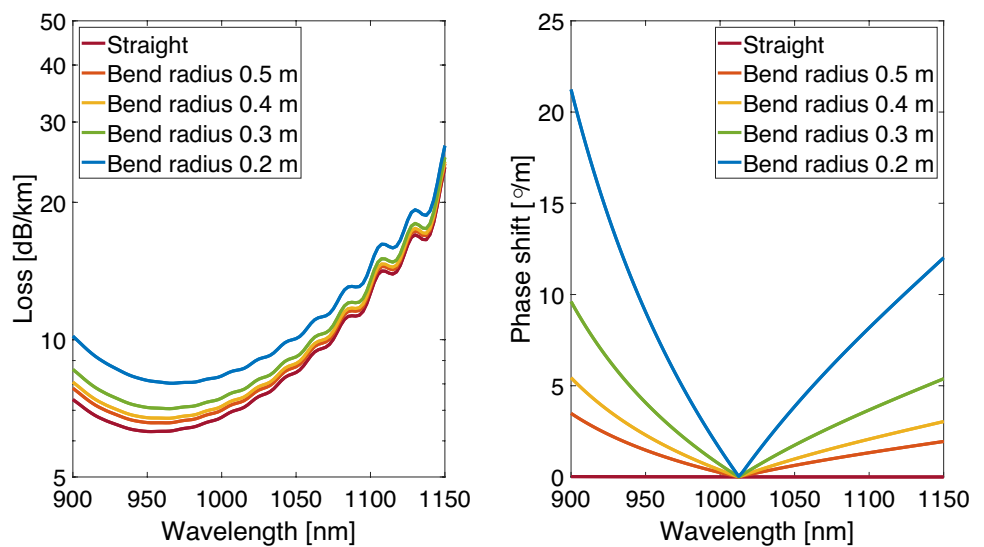


**Fig. 3** Computed phase shift between the two orthogonally polarized fundamental modes in tubular IC-HCPCFs at a bend radius of 0.2 m (see Fig. 1 the grey dashed line) with the design parameters given in Table 1. **a** Tubular IC-HCPCFs with a core diameter of 40

$\mu\text{m}$  and  $N=8$  capillaries. **b** Tubular IC-HCPCFs with a core diameter of 40  $\mu\text{m}$  and  $d_{\text{capillary}}/D_{\text{core}} = 0.377$ . **c** Tubular IC-HCPCFs with  $d_{\text{capillary}}/D_{\text{core}} = 0.377$  and  $N=8$  capillaries

is shown that this anti-resonant spectral position at which the phase shift is minimized can be shifted mainly by a proper choice of ratio  $d_{\text{capillary}}/D_{\text{core}}$

The influence of all design parameters of the fiber on the wavelength at which the phase shift between the two orthogonally polarized modes is minimized was investigated by the simulations. The strut thickness was kept constant at 736 nm to ensure the same spectral position of the transmission band and low losses of the fiber. The bending radius was set to the most critical value of 0.2 m (see Fig. 2). The three main parameters of the fiber are the core diameter  $D_{\text{core}}$ , the ratio  $d_{\text{capillary}}/D_{\text{core}}$  and the number of capillaries  $N$  (see Fig. 1). The different considered combinations are listed in Table 1. The simulation results for the bending-induced phase shift are shown in Fig. 3 while the corresponding confinement losses are shown in Fig. 4.

**Table 1** Set of parameters used to investigate the influence of the design of IC-HCPCFs on the bending-induced phase shift and on the confinement losses

Fiber design parameter	$d_{\text{capillary}}/D_{\text{core}}$	$N$	$D_{\text{core}} [\mu\text{m}]$
Starting point	0.377	8	40
Analysis 1	From 0.3 to 0.6	8	40
Analysis 2	0.377	From 7 to 9	40
Analysis 3	0.377	8	From 30 to 50

Figure 3a shows the calculated wavelength-dependent phase shift for a core diameter of  $D_{\text{core}} = 40\mu\text{m}$  and a cladding consisting of  $N = 8$  capillaries. Similar results are

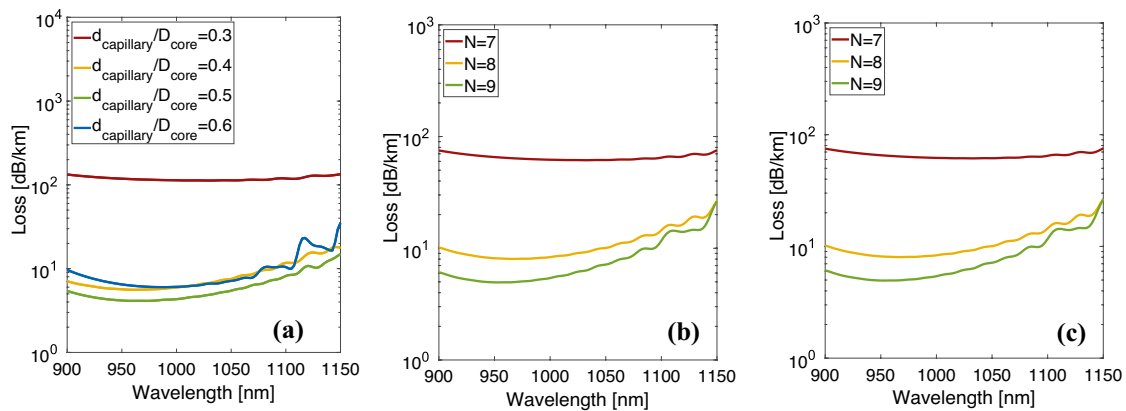


**Fig. 4** Confinement loss averaged over the two orthogonally polarized fundamental modes in tubular IC-HCPCFs at a bend radius of 0.2 m (see Fig. 1 the grey dashed line) with the design parameters given in Table 1. **a** Tubular IC-HCPCFs with a core diameter of 40

$\mu\text{m}$  and  $N=8$  capillaries. **b** Tubular IC-HCPCFs with a core diameter of 40  $\mu\text{m}$  and  $d_{\text{capillary}}/D_{\text{core}} = 0.377$ . **c** Tubular IC-HCPCFs with  $d_{\text{capillary}}/D_{\text{core}} = 0.377$  and  $N=8$  capillaries

obtained for the different ratios  $d_{\text{capillary}}/D_{\text{core}}$  with a slight shift to longer wavelengths as the ratio increases. Figure 4a depicts the corresponding confinement losses averaged over the two orthogonally polarized modes. The losses are only moderately affected by the ratio  $d_{\text{capillary}}/D_{\text{core}}$  as long as it is  $\geq 0.4$ , which means that the ratio  $d_{\text{capillary}}/D_{\text{core}}$  can be used as a design parameter to change the spectral position with the minimum phase shift between the orthogonally polarized modes (see Fig. 3a).

Figure 3b shows the impact that the number of capillaries has on the phase shift between the orthogonally polarized modes. Here the ratio  $d_{\text{capillary}}/D_{\text{core}}$  was set to 0.377 and the core diameter of the fiber is 40  $\mu\text{m}$ . Only fibers with 7, 8, or 9 capillaries were considered (bending orientation see Fig. 1) since  $N=6$  capillaries lead to excessive losses for the considered ratio  $d_{\text{capillary}}/D_{\text{core}}$  and  $N=10$  would require overlapping of the capillaries. Figure 4b shows the impact of the number of capillaries  $N$  on the confinement losses of tubular IC-HCPCFs. It can generally be concluded that the confinement is improved with an increasing number of capillaries in the fiber, but at the same time, this can also lead to efficient guiding of unwanted higher-order modes. The bending-induced phase shift increases more significantly with an increasing number of capillaries but fortunately has only a minor influence on the spectral position at which the phase shift is minimized. This minimum shifts to slightly shorter wavelengths with an increasing number of capillaries in the cladding.

To investigate the influence of the fiber's core diameter on the confinement loss and the bending-induced phase shift, the core diameter of the tubular IC-HCPCFs with 8 capillaries was varied from 30 to 50  $\mu\text{m}$  and the ratio  $d_{\text{capillary}}/D_{\text{core}}$  was kept again constant at 0.377. The results of the numerical simulations are shown in Fig. 3c. It is already known

from the literature [50] that the confinement loss is reduced with increasing core diameter since the overlap between guided modes and surrounding glass is reduced (see Fig. 4c). The bending-induced phase shift however increases significantly by enlarging the core and the spectral bandwidth for which the phase shift is below  $5^\circ/\text{m}$  is reduced from about 150 nm to nearly 30 nm when the core diameter is increased from 30 to 50  $\mu\text{m}$ .

## 4 Resulting fiber designs

Following the previous analysis, the design of a fiber suitable for PM transmission in the first step requires the specification of the operation wavelength which defines the required strut thickness as given by Eq. 1. After the choice of the desired core diameter  $D_{\text{core}}$  and the number of capillaries  $N$  to fulfill the requirement of a given application, the spectral position at which the phase shift is minimized can be flexibly tuned by varying the capillary diameter  $d_{\text{capillary}}$  which results in a change in the ratio of  $d_{\text{capillary}}/D_{\text{core}}$ . However, due to the nonexistence of a rigorous analytical model for the tubular IC-HCPCFs, the physical reason for this fact is still unclear and will be the subject of future work. Using this strategy, one can easily design a tubular IC-HCPCF to fulfill the requirement of PM transmission in an industrial environment, as discussed in the following.

According to ISO 11145:2018 (ISO.2018), a linearly polarized beam is defined by the degree of linear polarization (DOLP)  $> 90\%$ . Using this criterion, the fabrication tolerance was analyzed in the example of two proposed fiber designs. The Stokes formalism was used to retrieve the state of polarization of the beam after propagation through the fiber. The polarization state is represented by the Stokes

vector ( $\vec{S}$ ) which consists of the four Stokes parameters  $S_0, S_1, S_2,$  and  $S_3$ . The DOLP can be expressed as [51]

$$DOLP = \frac{\sqrt{S_1^2 + S_2^2}}{S_0}. \tag{3}$$

The change of the polarization state of the optical fiber can be described by a linear retarder using the Müller calculus using the corresponding  $4 \times 4$  Müller matrix [51]

$$M = \begin{bmatrix} 1 & 0 & 0 & 0 \\ 0 & \cos^2(2\theta) + \sin^2(2\theta)\cos(\Delta\delta) & \cos(2\theta)\sin(2\theta)(1 - \cos(\Delta\delta)) & \sin(2\theta)\sin(\Delta\delta) \\ 0 & \cos(2\theta)\sin(2\theta)(1 - \cos(\Delta\delta)) & \cos^2(2\theta)\cos(\Delta\delta) + \sin^2(2\theta) & -\cos(2\theta)\sin(\Delta\delta) \\ 0 & -\sin(2\theta)\sin(\Delta\delta) & \cos(2\theta)\sin(\Delta\delta) & \cos(\Delta\delta) \end{bmatrix} \tag{4}$$

where  $\Delta\delta$  represents the bending-induced phase shift and  $\theta$  is the angle between the bending plane of the optical fiber (see Fig. 1 grey dashed line) and the plane of polarization of the beam launched into the fiber (x-direction see Fig. 1d). Using a perfectly linearly polarized incident beam with a

polarization state  $\vec{S} = \begin{bmatrix} 1 \\ 1 \\ 0 \\ 0 \end{bmatrix}$ , the polarization state  $\vec{S}'$  after

transmission is given by

$$\vec{S}' = \begin{bmatrix} S'_0 \\ S'_1 \\ S'_2 \\ S'_3 \end{bmatrix} = M \cdot \vec{S} = M \cdot \begin{bmatrix} 1 \\ 1 \\ 0 \\ 0 \end{bmatrix} = \begin{bmatrix} 1 \\ \cos^2(2\theta) + \sin^2(2\theta)\cos(\Delta\delta) \\ \cos(2\theta)\sin(2\theta)(1 - \cos(\Delta\delta)) \\ -\sin(2\theta)\sin(\Delta\delta) \end{bmatrix}, \tag{5}$$

and the resulting DOLP is

$$DOLP = \sqrt{(\cos^2(2\theta) + \sin^2(2\theta)\cos(\Delta\delta))^2 + (\cos(2\theta)\sin(2\theta)(1 - \cos(\Delta\delta)))^2}. \tag{6}$$

When  $\theta$  is  $45^\circ$  or  $135^\circ$ , two orthogonally polarized modes are excited with equal power, which is the worst case since the change of the polarization state of the transmitted beam caused by bending-induced phase shift is maximal.

According to Eq. 6 the accumulated phase shift  $\Delta\delta$  after the optical fiber needs to be  $< 25.8^\circ$  to keep a DOLP of  $> 90\%$  for all possible orientations  $\theta$  of the polarization of the incident beam. For typical industrial applications of ultrashort laser pulses, the length of the fiber needs to be in the order of 10 m, from which it follows that the phase shift per unit length needs to be lower than  $2.58^\circ/\text{m}$ . This value was considered for the analysis of the fabrication tolerances.

A core diameter of  $40\mu\text{m}$  was chosen to ensure a confinement loss of the fundamental mode of less than 10 dB/km as well as a phase shift of less than  $2.58^\circ/\text{m}$  in a spectral range of several tens of nanometers around the anti-resonant wavelength for bend radii larger than 0.2 m. For fibers with a core diameter of  $30\mu\text{m}$  the required confinement loss of the fundamental mode cannot be achieved (see Fig. 4c). For fibers with a core diameter of  $50\mu\text{m}$ , the spectral bandwidth in which the phase shift is limited to  $2.58^\circ/\text{m}$  is too narrow (see Fig. 3c). Two PM

IC-HCPCFs consisting of a tubular structure with 7 and 8 capillaries designed for a wavelength of 1030 nm are proposed and discussed in the following. The two proposed fibers with 7 and 8 capillaries are labeled as T7 and T8 fibers, respectively. The ratio of  $d_{\text{capillary}}/D_{\text{core}}$  was optimized by the aforementioned method for both fibers. Their structures are shown by the insets of Fig. 5. The design parameters are given in Table 2.

To achieve a minimum phase shift at the wavelength of 1030 nm when the fiber is bent to a radius of 0.2 m, the ratio  $d_{\text{capillary}}/D_{\text{core}}$  was set to 0.524 and 0.553 for the T7 and the T8 fiber, respectively. Figure 5 shows the computed confinement loss averaged over the two orthogonally polarized fundamental modes and the resulting phase shift for bend radii ranging from 0.1 to 0.5 m for the two fibers. Both fibers exhibit low confinement losses of less than 10 dB/km for bending radii exceeding 0.15 m and the phase shift is less than  $0.05^\circ/\text{m}$  for bending radii ranging from 0.18 to 0.5 m, which shows the promising PM potential using these fibers. The wavelength-dependent confinement loss and bending-induced phase shift of the fundamental modes in the two fibers with a bending

radius of 0.2 m are shown in Fig. 6. The fibers show losses of less than 10 dB/km for a spectral region ranging from 900 to 1125 nm. The spectral bandwidth in which the bending-induced phase shift is below  $2.58^\circ/\text{m}$  amounts to over 35 nm with a minimized phase shift at 1030 nm.

This result confirms our previous analysis and shows great potential to implement PM tubular IC-HCPCFs using a low-birefringence approach (corresponding to a modal birefringence parameter  $< 7 \times 10^{-9}$ ) by tuning a single design parameter  $d_{\text{capillary}}/D_{\text{core}}$  instead of intentionally modifying the structure of the fiber's cladding to enhance the birefringence. The two proposed fibers fulfill the requirements of

**Fig. 5** Confinement losses averaged over the two orthogonally polarized fundamental modes (a) and bending-induced phase shift between the two orthogonally polarized fundamental modes (b) as a function of the bending radius for the two proposed fibers for a perfectly linearly polarized incident beam with an orientation angle  $\theta$  of  $45^\circ$  or  $135^\circ$ . (T7 fiber:  $D_{core} = 40\mu\text{m}$ ,  $d_{capillary}/D_{core} = 0.524$ ,  $N = 7$  capillaries and T8 fiber:  $D_{core} = 40\mu\text{m}$ ,  $d_{capillary}/D_{core} = 0.553$ ,  $N = 8$  capillaries)

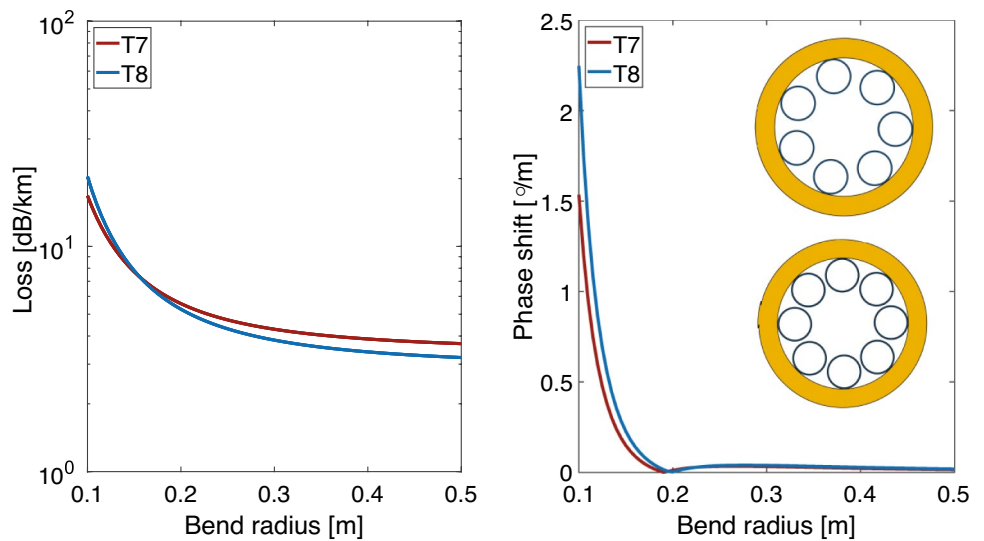


**Table 2** Summary of design parameters of the proposed PM tubular IC-HCPCFs

Fiber design parameter	$d_{capillary}/D_{core}$	$N$	$D_{core}[\mu\text{m}]$
T7	0.524	7	40
T8	0.553	8	40

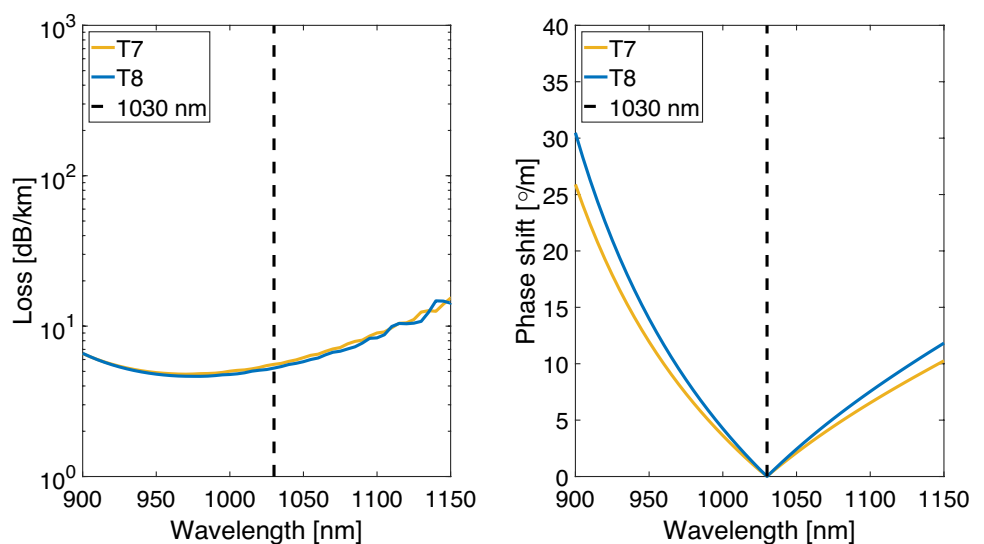
PM transmission with low losses for an ideal structure. In the production however one needs to consider small deviations from the ideal structure, as discussed in the following.

### 5 Analysis of fabrication tolerances

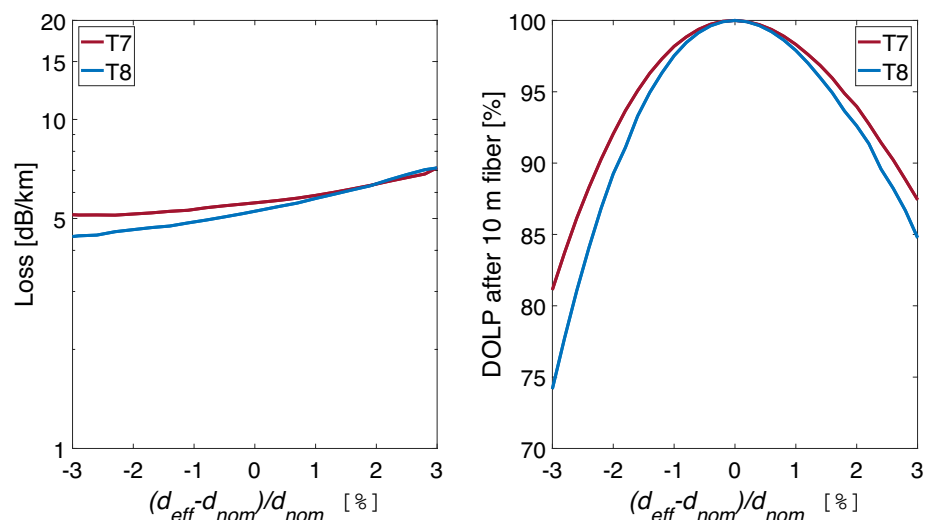
Due to the conservation of mass, the cross-sectional area of the thin glass walls of the capillaries (see blue parts in

Fig. 1) stays constant during the fiber production process when the preform exhibits a uniform structure along its whole length and a constant ratio between the feeding and the pulling velocities is ensured. The diameter of the capillaries in the fiber is adjusted by applying pressure to the capillaries during the drawing process. A higher pressure applied to the capillaries leads to larger capillary diameters and a smaller strut thickness and vice versa. Due to small deviations from the target process parameters during manufacturing, the capillary properties can deviate from the design which leads to a detrimental influence on the PM behavior of the fiber. Figure 7 shows the influence of the fluctuation of the capillary’s diameter on the resulting DOLP for a fiber with a length of 10 m at a wavelength of 1030 nm and a bending radius of 0.2 m (bending orientation see Fig. 1). The relative deviation of the diameters is defined as  $(d_{eff} - d_{nom})/d_{nom}$ , where the  $d_{eff}$  and  $d_{nom}$  are the effective

**Fig. 6** Confinement loss averaged over the two orthogonally polarized fundamental modes (a) and bending-induced phase shift of fundamental modes (b) as a function of the wavelength for a perfectly linearly polarized incident beam with orientation angle  $\theta$  of  $45^\circ$  or  $135^\circ$ ; the bending radius was set to 0.2 m (see Fig. 1 the grey dashed line); T7 fiber:  $D_{core} = 40\mu\text{m}$ ,  $d_{capillary}/D_{core} = 0.524$ ,  $N = 7$  capillaries; T8 fiber:  $D_{core} = 40\mu\text{m}$ ,  $d_{capillary}/D_{core} = 0.553$ ,  $N = 8$  capillaries



**Fig. 7** Confinement loss averaged over the two orthogonally polarized fundamental modes (a) and resulting DOLP after 10 m of fiber (b) as a function of the relative deviation of the effective diameter of the fiber from its nominal value  $(d_{eff} - d_{nom})/d_{nom}$  in case of a perfectly linearly polarized incident beam with orientation angle  $\theta$  of  $45^\circ$  or  $135^\circ$  and bending radius of 0.2 m (see Fig. 1 the grey dashed line) and a wavelength of 1030 nm for two proposed tubular IC-HCPCF designs



and nominal outer diameters of the capillaries, respectively. While keeping a constant cross-sectional area of the glass walls of the capillaries (see blue parts in Fig. 1), the relative deviation varied from  $-3\%$  ( $d_{eff}$  about  $20.32 \mu\text{m}$  for T7 and  $21.44 \mu\text{m}$  for T8 fiber) to  $+3\%$  ( $d_{eff}$  about  $21.58 \mu\text{m}$  for T7 and  $22.76 \mu\text{m}$  for T8 fiber). For all resulting fibers, a loss of less than 10 dB/km was observed with only small changes compared to the values of the nominal design (see Fig. 7a). The DOLP after 10 m of fiber however drops significantly with larger deviations from the nominal design ( $d_{eff}$  about  $20.96 \mu\text{m}$  for T7 and  $22.12 \mu\text{m}$  for T8 fiber). The acceptable relative deviation (DOLP  $> 90\%$  after 10 m of fiber) of the capillary diameter is found to range between  $-2.2\%$  ( $d_{eff} = 20.49 \mu\text{m}$ ) and  $+2.6\%$  ( $d_{eff} = 21.5 \mu\text{m}$ ) for T7, while the tolerances are even tighter for the T8 fiber where the diameter

of the fiber should not vary for more than  $-1.9\%$  ( $d_{eff} = 21.68 \mu\text{m}$ ) to  $+2.3\%$  ( $d_{eff} = 22.61 \mu\text{m}$ ).

After considering a uniform change of all capillaries, we now discuss the impact of a gradient of the diameters of the capillaries in the fiber's cross-section from one side to the opposite side, which can be often observed in produced fibers. The resulting fiber cross-sections are shown in Fig. 8c where the gradient has been exaggerated for a better visualization. The gradient of the capillary diameters leads to non-uniform gaps between neighboring capillaries and can easily be caused by imprecise pressurization of the capillaries during the production of the fiber (Nawazuddin et al. 2018). As mentioned before, due to a constant cross-sectional area of the thin membranes of the glass capillaries (see blue parts in Fig. 1), the variation of the capillary diameters can lead to

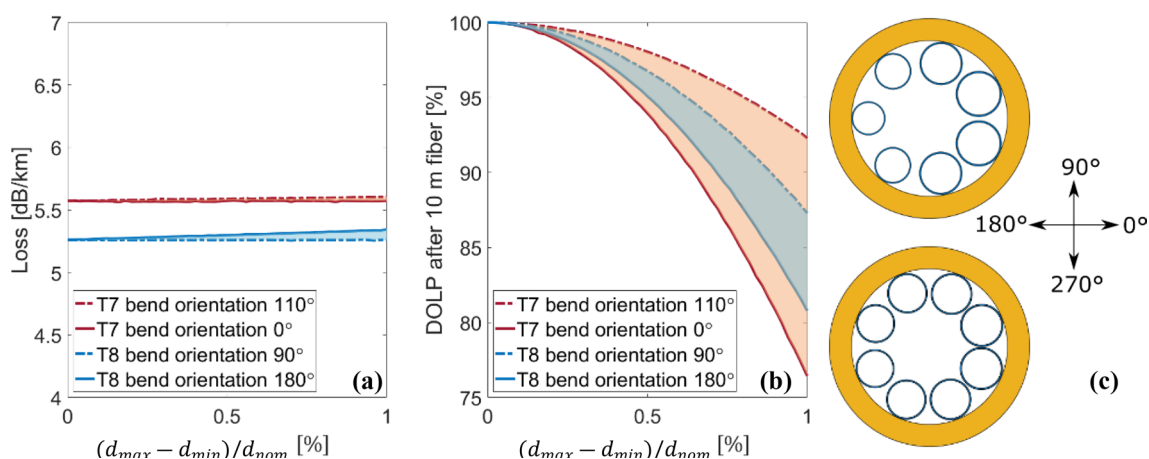


**Fig. 8** Confinement loss averaged over the two orthogonally polarized fundamental modes (a) and resulting DOLP after 10 m output of the fiber (b) as a function of normalized difference  $(d_{max} - d_{min})/d_{nom}$  of the maximum and minimum diameters of the capillaries in the fibers for two tubular IC-HCPCF designs with a bending radius of 0.2

m and a wavelength of 1030 nm for a perfectly linearly polarized incident beam with orientation angle  $\theta$  of  $45^\circ$  or  $135^\circ$ . The varying diameters of the capillaries is sketched in c which also indicates the reference for the bending directions



unequal strut thicknesses. This asymmetry of the fiber structure and the resulting variation of the strut thickness can lead to a narrowing of the transmission band and a dependence on the bending-induced phase shift as well as the losses on the orientation of the bending.

Figure 8 shows the computed confinement losses averaged over the two orthogonally polarized fundamental modes and the resulting DOLP after propagation through 10 m of fiber with a bend radius of 0.2 m for different bending orientations while keeping a constant angle  $\theta = 45^\circ$  or  $135^\circ$  of the polarization direction. In this case, the normalized deviation of the capillary diameters is defined as  $(d_{max} - d_{min})/d_{nom}$ , where the  $d_{max}$ ,  $d_{min}$  and  $d_{nom}$  are the largest, the smallest, and the nominal value of the outer diameters of the capillaries for each fiber. While only slight changes in the confinement loss for different bending orientations are observed, the phase shift strongly depends on the bending orientation (see Fig. 8). The bending orientations with maximal DOLP (hence minimal degradation of the DOLP) are  $110^\circ$  for the T7 fiber and  $90^\circ$  for the T8 fiber, while the bending orientations resulting in a minimal DOLP are  $0^\circ$  and  $180^\circ$ , respectively. The dashed and solid curves show the limit of the maximal and minimal DOLP of the two fibers, whereas the shaded areas show the influence of different bending orientations. The degradation of the polarization is significantly enhanced when the normalized deviation of the capillary size increases, while the confinement losses are almost constant. This leads to very tight tolerances of the fabrication with a maximum allowed deviation of 0.64% from the original design for both tubular IC-HCPCFs to achieve the target DOLP of  $> 90\%$ . This is very challenging for fiber production. With the tremendous development of the technologies for the fabrication of hollow-core fibers, new approaches have emerged, such as the direct drawing of fibers from the stacked-cane preform using the stack, seal, evacuate, and draw technique [52]. The fabrication of tubular IC-HCPCFs with a nearly perfect symmetrical structure is feasible by using the new fabrication techniques combined with the separate control of each glass capillary during the pressurization. With precise control of the drawing parameters, it is also feasible to maintain the rather large strut thickness of around 736 nm and the size of the glass capillaries along the fiber length. Another way to mitigate this narrow fabrication tolerance is the reduction of the fiber length. Figure 9 shows the fabrication tolerance of the two proposed fiber designs regarding the normalized deviation of the capillary diameters as a function of the fiber length, after which the DOLP of the output beam is larger than 90%. This shows the trade-off between the fabrication tolerance of the two proposed fiber designs and the fiber length, after which the requirement can be fulfilled. The fabrication tolerance increases to 1.2% for 5 m of fiber, while this value is more than 6% for the fiber with a length of 1 m. This will ease the challenging

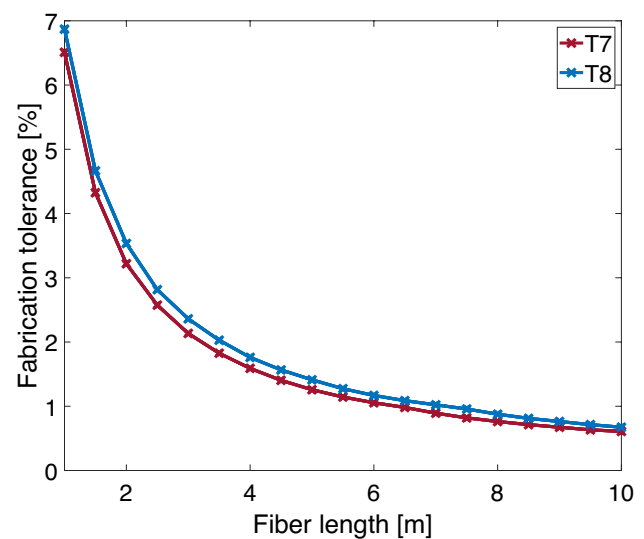


**Fig. 9** Fabrication tolerance of the two proposed fiber designs regarding the normalized difference  $(d_{max} - d_{min})/d_{nom}$  of the capillary diameters as a function of the fiber length, after which the DOLP of the output beam is larger than 90%

task of fiber fabrication. It is worth mentioning that the frozen twist introduced during fiber fabrication is commonly known to enhance the birefringence of IC-HCPCFs [53, 54]. According to the work of Röhrer [42], this twist effect was found to be negligible for the limited fiber length of 10 m. Despite our analysis not encompassing all possible variations, the fabrication imperfection due to the non-equal size of the glass capillaries shown in Fig. 8 was found to be the most critical factor concerning the fabrication tolerance.

## 6 Conclusion

In summary, a theoretical analysis was conducted to investigate the influence of the essential design parameters on the bending-induced phase shift in inhibited-coupling hollow-core photonic-crystal fibers (IC-HCPCFs). The possibility of realizing polarization-maintaining (PM) IC-HCPCFs using a tubular structure has been discussed. Two designs of tubular IC-HCPCFs with 7 and 8 glass capillaries were proposed for a PM operation at a wavelength of 1030 nm. Numerical simulation showed low guiding losses and a PM behavior. The resulting degree of linear polarization (DOLP) was larger than 90% after propagating through 10 m of fiber with a bend radius larger than 0.2 m. These designs show great potential for the delivery of linearly polarized beams with high intensity. Our comprehensive analysis has however also revealed tight fabrication tolerances and that even small deviations from the ideal fiber structures lead to an enhancement of the modal birefringence. Precise control of

the drawing parameters during fiber production is therefore needed.

**Acknowledgements** This work was supported by the Landesministerium für Wissenschaft, Forschung und Kunst Baden-Württemberg (Ministry of Science, Research and the Arts of the State of Baden-Württemberg) within the Nachhaltigkeitsförderung (sustainability support) of the projects of the Exzellenzinitiative II.

**Author contributions** BC conducted the theoretical investigations and wrote the manuscript. TK and CR participated in the theoretical investigations. TG and MAA assisted in the preparation of the manuscript. All authors reviewed the manuscript.

**Funding** Open Access funding enabled and organized by Projekt DEAL. Funding was provided by Landesministerium für Wissenschaft, Forschung und Kunst Baden-Württemberg (Ministry of Science, Research and the Arts of the State of Baden-Württemberg) within the Nachhaltigkeitsförderung (sustainability support) of the projects of the Exzellenzinitiative II.

**Data availability** The data that support the findings of this study are available from the corresponding author, B. Chen, upon reasonable request.

## Declarations

**Competing interests** The authors declare no competing interests.

**Open Access** This article is licensed under a Creative Commons Attribution 4.0 International License, which permits use, sharing, adaptation, distribution and reproduction in any medium or format, as long as you give appropriate credit to the original author(s) and the source, provide a link to the Creative Commons licence, and indicate if changes were made. The images or other third party material in this article are included in the article's Creative Commons licence, unless indicated otherwise in a credit line to the material. If material is not included in the article's Creative Commons licence and your intended use is not permitted by statutory regulation or exceeds the permitted use, you will need to obtain permission directly from the copyright holder. To view a copy of this licence, visit <http://creativecommons.org/licenses/by/4.0/>.

## References

1. A. Börzsönyi, Z. Heiner, M.P. Kalashnikov, A.P. Kovács, K. Osvay, Dispersion measurement of inert gases and gas mixtures at 800 nm. *Appl. Opt.* **47**, 4856–4863 (2008). <https://doi.org/10.1364/AO.47.004856>
2. H. Sakr, Y. Chen, G.T. Jasion, T.D. Bradley, J.R. Hayes, H.C.H. Mulvad, I.A. Davidson, E. NumkamFokoua, F. Poletti, Hollow core optical fibres with comparable attenuation to silica fibres between 600 and 1100 nm. *Nat. Commun.* **11**, 6030 (2020). <https://doi.org/10.1038/s41467-020-19910-7>
3. P.J. Roberts, F. Couny, H. Sabert, B.J. Mangan, D.P. Williams, L. Farr, M.W. Mason, A. Tomlinson, T.A. Birks, J.C. Knight, P.S.J. Russell, Ultimate low loss of hollow-core photonic crystal fibres. *Opt. Express* **13**, 236–244 (2005). <https://doi.org/10.1364/OPEX.13.000236>
4. F. Poli, A. Cucinotta, S. Selleri, *Photonic crystal fibers: properties and applications* (Springer, Netherlands, 2007)
5. T.A. Birks, J.C. Knight, P.J. St. Russell, Endlessly single-mode photonic crystal fiber. *Opt. Lett.* **22**, 961–963 (1997). <https://doi.org/10.1364/OL.22.000961>
6. J.C. Knight, T.A. Birks, P.J. St. Russell, D.M. Atkin, All-silica single-mode optical fiber with photonic crystal cladding. *Opt. Lett.* **21**, 1547–1549 (1996). <https://doi.org/10.1364/OL.21.001547>
7. B.J. Mangan, L. Farr, A. Langford, P.J. Roberts, D.P. Williams, F. Couny, M. Lawman, M. Mason, S. Coupland, R. Flea, H. Sabert, T.A. Birks, J.C. Knight, P.S.J. Russell, Low loss (1.7 dB/km) hollow core photonic bandgap fiber, in: *Optical Fiber Communication Conference, 2004. OFC 2004, 2004*, 3 p vol.2.
8. G. Humbert, J.C. Knight, G. Bouwmans, P.J. StRussell, D.P. Williams, P.J. Roberts, B.J. Mangan, Hollow core photonic crystal fibers for beam delivery. *Opt. Express* **12**, 1477–1484 (2004). <https://doi.org/10.1364/OPEX.12.001477>
9. F. Benabid, J. Knight, G. Antonopoulos, P. Russell, Stimulated Raman scattering in hydrogen-filled hollow-core photonic crystal fiber. *Science* **298**, 399–402 (2002). <https://doi.org/10.1126/science.1076408>
10. B. Debord, A. Amsanpally, M. Chafer, A. Baz, M. Maurel, J.M. Blondy, E. Hugonnot, F. Scol, L. Vincetti, F. Gérôme, F. Benabid, Ultralow transmission loss in inhibited-coupling guiding hollow fibers. *Optica* **4**, 209–217 (2017). <https://doi.org/10.1364/OPTICA.4.000209>
11. Y.Y. Wang, X. Peng, M. Alharbi, C.F. Duting, T.D. Bradley, F. Gérôme, M. Mielke, T. Booth, F. Benabid, Design and fabrication of hollow-core photonic crystal fibers for high-power ultrashort pulse transportation and pulse compression. *Opt. Lett.* **37**, 3111–3113 (2012). <https://doi.org/10.1364/OL.37.003111>
12. B. Debord, F. Amrani, L. Vincetti, F. Gérôme, F. Benabid, Hollow-core fiber technology: the rising of “Gas Photonics.” *Fibers* **7**, 16 (2019). <https://doi.org/10.3390/fib7020016>
13. B. Debord, F. Gérôme, P.-M. Paul, A. Husakou, F. Benabid, 2.6 mJ energy and 81 GW peak power femtosecond laser-pulse delivery and spectral broadening in inhibited coupling Kagome fiber, in: *CLEO: 2015, Optica Publishing Group, 2015*, STh4L.7.
14. P. Uebel, M.C. Günendi, M.H. Frosz, G. Ahmed, N.N. Edavalath, J.-M. Ménard, P.S.J. Russell, Broadband robustly single-mode hollow-core PCF by resonant filtering of higher-order modes. *Opt. Lett.* **41**, 1961–1964 (2016). <https://doi.org/10.1364/OL.41.001961>
15. J.R. Hayes, S.R. Sandoghchi, T.D. Bradley, Z. Liu, R. Slavík, M.A. Gouveia, N.V. Wheeler, G. Jasion, Y. Chen, E.N. Fokoua, M.N. Petrovich, D.J. Richardson, F. Poletti, Antiresonant Hollow Core Fiber with Octave Spanning Bandwidth for Short Haul Data Communications, in: *Optical Fiber Communication Conference Postdeadline Papers, Optica Publishing Group, 2016*, Th5A.3.
16. K.F. Mak, J.C. Travers, P. Hölzer, N.Y. Joly, P.J. St. Russell, Tunable vacuum-UV to visible ultrafast pulse source based on gas-filled Kagome-PCF. *Opt. Express* **21**, 10942–10953 (2013). <https://doi.org/10.1364/OE.21.010942>
17. H. Schmidt, A. Hawkins, Atomic spectroscopy and quantum optics in hollow-core waveguides. *Laser Photonics Rev.* **4**, 720–737 (2010). <https://doi.org/10.1002/lpor.200900040>
18. M.S. Ferreira, J. Bierlich, J. Kobelke, J.L. Pinto, K. Wondraczek, Negative curvature hollow core fiber sensor for the measurement of strain and temperature. *Opt. Express* **29**, 5808–5818 (2021). <https://doi.org/10.1364/OE.412532>
19. M. Michieletto, J.K. Lyngsø, C. Jakobsen, J. Lægsgaard, O. Bang, T.T. Alkeskjold, Hollow-core fibers for high power pulse delivery. *Opt. Express* **24**, 7103–7119 (2016). <https://doi.org/10.1364/OE.24.007103>
20. W. Schulz, U. Eppelt, R. Poprawe, Review on laser drilling I. Fundamentals, modeling, and simulation. *J. Laser Appl.* **25**, 12006 (2013)

21. C. Freitag, M. Wiedenmann, J.P. Negel, A. Loescher, V. Onuseit, R. Weber, M. Abdou Ahmed, T. Graf, High-quality processing of CFRP with a 1.1-kW picosecond laser. *Appl. Phys. A* **119**, 1237–1243 (2015). <https://doi.org/10.1007/s00339-015-9159-3>
22. P. Bizi-bandoki, S. Valette, E. Audouard, S. Benayoun, Time dependency of the hydrophilicity and hydrophobicity of metallic alloys subjected to femtosecond laser irradiations. *Appl. Surf. Sci.* **273**, 399–407 (2013). <https://doi.org/10.1016/j.apsusc.2013.02.054>
23. A.-M. Kietzig, S.G. Hatzikiriakos, P. Englezos, Patterned superhydrophobic metallic surfaces. *Langmuir* **25**, 4821–4827 (2009). <https://doi.org/10.1021/la8037582>
24. Y. Wang, M. Alharbi, T.D. Bradley, C. Fourcade-Dutin, B. Debord, F. Beaudou, F. Gérôme, F. Benabid, Hollow-core photonic crystal fiber for high power laser beam delivery. *High Power Laser Sci. Eng.* **1**, 17–28 (2013). <https://doi.org/10.1017/hpl.2013.3>
25. T.G. Helmut Hügel, *Materialbearbeitung mit Laser: Grundlagen und Verfahren*, 5th edn. (Springer, Wiesbaden, 2023)
26. I. Kaminow, Polarization in optical fibers. *IEEE J. Quantum Electron.* **17**, 15–22 (1981). <https://doi.org/10.1109/JQE.1981.1070626>
27. J. Noda, K. Okamoto, Y. Sasaki, Polarization-maintaining fibers and their applications. *J. Lightwave Technol.* **4**, 1071–1089 (1986). <https://doi.org/10.1109/JLT.1986.1074847>
28. F. Mitschke, *Fiber optics: physics and technology* (Springer, Berlin Heidelberg, 2010)
29. X. Chen, M.-J. Li, N. Venkataraman, M.T. Gallagher, W.A. Wood, A.M. Crowley, J.P. Carberry, L.A. Zenteno, K.W. Koch, Highly birefringent hollow-core photonic bandgap fiber. *Opt. Express* **12**, 3888–3893 (2004). <https://doi.org/10.1364/OPEX.12.003888>
30. P.J. Roberts, D.P. Williams, H. Sabert, B.J. Mangan, D.M. Bird, T.A. Birks, J.C. Knight, P.J. St Russell, Design of low-loss and highly birefringent hollow-core photonic crystal fiber. *Opt. Express* **14**, 7329–7341 (2006). <https://doi.org/10.1364/OE.14.007329>
31. J.M. Fini, J.W. Nicholson, B. Mangan, L. Meng, R.S. Windeler, E.M. Monberg, A. DeSantolo, F.V. DiMarcello, K. Mukasa, Polarization maintaining single-mode low-loss hollow-core fibres. *Nat. Commun. Commun.* **5**, 5085 (2014). <https://doi.org/10.1038/ncomms6085>
32. L. Vincetti, V. Setti, Elliptical hollow core tube lattice fibers for terahertz applications. *Opt. Fiber Technol.* **19**, 31–34 (2013). <https://doi.org/10.1016/j.yofte.2012.09.008>
33. S.A. Mousavi, S.R. Sandoghchi, D.J. Richardson, F. Poletti, Broadband high birefringence and polarizing hollow core antiresonant fibers. *Opt. Express* **24**, 22943–22958 (2016). <https://doi.org/10.1364/OE.24.022943>
34. W. Ding, Y.-Y. Wang, Hybrid transmission bands and large birefringence in hollow-core anti-resonant fibers. *Opt. Express* **23**, 21165–21174 (2015). <https://doi.org/10.1364/OE.23.021165>
35. C. Wei, C.R. Menyuk, J. Hu, Polarization-filtering and polarization-maintaining low-loss negative curvature fibers. *Opt. Express* **26**, 9528–9540 (2018). <https://doi.org/10.1364/OE.26.009528>
36. S. Yan, S. Lou, W. Zhang, Z. Lian, Single-polarization single-mode double-ring hollow-core anti-resonant fiber. *Opt. Express* **26**, 31160–31171 (2018). <https://doi.org/10.1364/OE.26.031160>
37. X. Zhao, J. Xiang, X. Wu, Z. Li, High birefringence, single-polarization, low loss hollow-core anti-resonant fibers. *Opt. Express* **29**, 36273–36286 (2021). <https://doi.org/10.1364/OE.439550>
38. G. Stępniewski, D. Dobrakowski, D. Pysz, R. Kasztelaniec, R. Buczyński, M. Klimczak, Birefringent large-mode-area anti-resonant hollow core fiber in the 1.9  $\mu\text{m}$  wavelength window. *Opt. Lett.* **45**, 4280–4283 (2020). <https://doi.org/10.1364/OL.398650>
39. Y.-F. Hong, Highly birefringent anti-resonant hollow-core fiber with a bi-thickness fourfold semi-tube structure. *Laser Photon. Rev.* **16**, 2100365 (2022)
40. A. Taranta, E. NumkamFokoua, S. AbokhamisMousavi, J.R. Hayes, T.D. Bradley, G.T. Jasion, F. Poletti, Exceptional polarization purity in antiresonant hollow-core optical fibres. *Nat. Photon.* **14**, 504–510 (2020). <https://doi.org/10.1038/s41566-020-0633-x>
41. M. Maurel, M. Chafer, A. Amsanpally, M. Adnan, F. Amrani, B. Debord, L. Vincetti, F. Gérôme, F. Benabid, Optimized inhibited-coupling Kagome fibers at Yb-Nd: Yag (8.5 dB/km) and Ti: Sa (30 dB/km) ranges. *Opt. Lett.* **43**, 1598–1601 (2018). <https://doi.org/10.1364/OL.43.001598>
42. C. Röhrer, J.H. Osório, F. Beirrow, M. Maurel, B. Debord, T. Graf, F. Gérôme, F. Benabid, M. Abdou Ahmed, Phase shift induced degradation of polarization caused by bends in inhibited-coupling guiding hollow-core fibers. *IEEE Photon. Technol. Lett.* **31**, 1362–1365 (2019). <https://doi.org/10.1109/LPT.2019.2927046>
43. Y.Y. Wang, F. Couny, P.J. Roberts, F. Benabid, Low loss broadband transmission in optimized core-shape Kagome Hollow-Core PCF, in: *Conference on Lasers and Electro-Optics 2010*, Optica Publishing Group, 2010, CPDB4.
44. S.-F. Gao, Y.-Y. Wang, W. Ding, D.-L. Jiang, S. Gu, X. Zhang, P. Wang, Hollow-core conjoined-tube negative-curvature fibre with ultralow loss. *Nat. Commun. Commun.* **9**, 2828 (2018). <https://doi.org/10.1038/s41467-018-05225-1>
45. M. Abdou-Ahmed, A. Voss, Optical fibres for high-power single-mode beam delivery. *Optik & Photonik* **7**, 38–43 (2012). <https://doi.org/10.1002/opph.201290046>
46. J.-P. Berenger, A perfectly matched layer for the absorption of electromagnetic waves. *J. Comput. Phys.* **114**, 185–200 (1994). <https://doi.org/10.1006/jcph.1994.1159>
47. R.T. Schermer, J.H. Cole, Improved bend loss formula verified for optical fiber by simulation and experiment. *IEEE J. Quantum Electron.* **43**, 899–909 (2007). <https://doi.org/10.1109/JQE.2007.903364>
48. A.N. Kolyadin, A.F. Kosolapov, A.D. Pryamikov, A.S. Biriukov, V.G. Plotnichenko, E.M. Dianov, Light transmission in negative curvature hollow core fiber in extremely high material loss region. *Opt. Express* **21**, 9514–9519 (2013). <https://doi.org/10.1364/OE.21.009514>
49. V. Zuba, H.C.H. Mulvad, R. Slavík, H. Sakr, F. Poletti, D.J. Richardson, E.N. Fokoua, Limits of coupling efficiency into hollow-core antiresonant fibres. *J. Lightwave Technol.* **41**, 6374–6382 (2023). <https://doi.org/10.1109/JLT.2023.3279701>
50. L. Vincetti, Empirical formulas for calculating loss in hollow core tube lattice fibers. *Opt. Express* **24**, 10313–10325 (2016). <https://doi.org/10.1364/OE.24.010313>
51. E. Collett, *Field guide to polarization*, society of photo optical, 2005.
52. L.R. Murphy, S. Yerolatsitis, T.A. Birks, J.M. Stone, Stack, seal, evacuate, draw: a method for drawing hollow-core fiber stacks under positive and negative pressure. *Opt. Express* **30**, 37303–37313 (2022). <https://doi.org/10.1364/OE.470599>
53. S.F. Feldman, D.A. Weinberger, H.G. Winful, Polarization instability in a twisted birefringent optical fiber. *J. Opt. Soc. Am. B* **10**, 1191–1201 (1993). <https://doi.org/10.1364/JOSAB.10.001191>
54. P. Roth, Y. Chen, M.C. Günendi, R. Beravat, N.N. Edavalath, M.H. Frosz, G. Ahmed, G.K.L. Wong, P.J. St Russell, Strong circular dichroism for the HE<sub>11</sub> mode in twisted single-ring hollow-core photonic crystal fiber. *Optica* **5**, 1315–1321 (2018). <https://doi.org/10.1364/OPTICA.5.001315>

**Publisher's Note** Springer Nature remains neutral with regard to jurisdictional claims in published maps and institutional affiliations.